

Investigation of Co₃Mo and Co₆Mo₇ binary alloys as electrocatalysts for hydrogen evolution reaction in acidic media

Youyi Sun and Alexey Y. Ganin*

School of Chemistry, University of Glasgow, Glasgow, G12 8QQ, UK

* Correspondence: alexey.ganin@glasgow.ac.uk; Tel.: +44-0141-330-8404

Received: date; Accepted: date; Published: date

Abstract: Metal alloys have become ubiquitous choice as catalysts for electrochemical hydrogen evolution in alkaline media. However, scarce and expensive Pt remains the key electrocatalyst in acidic electrolytes making the search for earth-abundant and cheaper alternatives appealing. Herein, we present a facile and efficient synthetic route towards polycrystalline Co₃Mo and Co₆Mo₇ metal alloys that achieve competitively low overpotentials of 115 mV and 160 mV at 10 mA cm⁻² in 0.5 M H₂SO₄. Both alloys outperform Co and Mo metals which showed significantly higher overpotentials and lower current densities when tested under identical conditions. However, the low overpotential in Co₃Mo comes at the price of stability. It rapidly becomes inactive when tested under applied potential bias. On the other hand, Co₇Mo₆ retains the current density over time without the evidence of current decay. The findings demonstrate that even in free-standing form and without nanostructuring polycrystalline bimetallic electrocatalysts could challenge the dominance of Pt in the acidic media if the ways for improving their stability were found.

Keywords: Hydrogen evolution reaction; Metal alloys; Water electrolysis; Acidic Conditions

1. Introduction

The share of wind and solar in a global electricity output has reached 9 % in Q1 2020 [1]. It is largely anticipated that the output from renewables will continue to grow over next decade. This presents a substantial challenge to distribution networks due to the intermittent nature of renewable energy. Batteries have been considered as an efficient way for moderating the daily change in electricity production, but they discharge quickly and hence, are currently unable to provide a long-term solution for managing the electricity output between the seasons [2]. Storing the excess of renewable electricity directly as fuels, for example, from photovoltaic cells during summer and then use these fuels later during cold and short winter days could be a practical way to address this challenge.

Hydrogen (with a world demand of over 70 Mt per year in 2018 [3]) is an excellent fuel and key feedstock in the production of chemicals and fertilisers. However, less than 0.1 % of global hydrogen currently comes from water electrolysis. This can change rapidly if electrolysis is used as a storage platform for mitigating seasonal variations in electricity output rather than a stand-alone method of H₂ production [4]. In an electrochemical cell (which is an integral part of any industrial electrolyser) water electrolysis yields best results in alkaline and acidic electrolytes. Hydrogen evolves at a cathode and thus, the choice of cathode materials (which simultaneously act as electrocatalysts) is crucial for driving the hydrogen evolution reaction (HER) from water at appreciable voltage and current density rates [5]. Industrial alkaline electrolysers (AEL) with an energy output as high as 6 MW [4] have already benefited from the early adaptation of low-cost Ni-based alloys as cathode materials [6, 7]. Pt-group metals, on the other hand, still remain the only viable choice in acidic conditions [8]. Platinum contributes to the costs of proton-exchange membrane electrolysers (PEMEL) which are almost twice as expensive per KWh as AEL [4]. With the PEMEL offering short start-up times and load-flexibility (important parameters for the integration with renewable energy networks) reducing the cost of PEMEL is important. Finding earth-abundant alternatives to Pt in acidic conditions is thus, seems to be

a key to future integration of PEMEL into renewable networks and more research is needed in this context.

Metal alloys show electrocatalytic performance superior to their individual metal counterparts [9]. This synergetic effect has been successfully exploited in alkaline electrolytes [4, 6] but only limited attempts have been made to investigate polycrystalline products with well-defined structures and compositions in acidic media [10]. A growing interest in nanostructured materials appeals for a better understanding of the electrochemical properties of pure-phased polycrystalline alloys and in this respect Co – Mo system remains relatively unexplored. Coupled with the recent reports of impressive performance of Co_3Mo towards HER in 1M KOH [11, 12], the investigation of electrochemical properties of alloys in the Co – Mo system under acidic condition is key to understanding how cheaper and more efficient electrocatalysts could be designed and made.

In this work we investigated two binary compounds within the Co – Mo system and tested them as electrocatalysts for HER in acidic conditions. Phase-pure, polycrystalline Co_3Mo and Co_7Mo_6 were prepared as powders and electrochemically tested for HER in acidic and alkaline media. The tests were carried out on free-standing products directly on a glassy carbon electrode to minimize the effect of the substrate and possible impurities on their catalytic performance and electrochemical stability. There was a pronounced synergistic effect for both Co_3Mo and Co_6Mo_7 that showed substantially higher current densities compared with Co and Mo metals. However, polycrystalline free-standing Co_3Mo has a poor electrochemical stability which makes it suboptimal choice compared with Co_7Mo_6 which retained its performance after prolonged hours of testing.

2. Experimental Section

2.1. Synthesis

CoMoO_4 precursor was made from $\text{Na}_2\text{MoO}_4 \cdot 2\text{H}_2\text{O}$ (Aldrich, 99.99 %) and $\text{CoCl}_2 \cdot 6\text{H}_2\text{O}$ (Alfa Aesar, 99.9 %). First, $\text{Na}_2\text{MoO}_4 \cdot 2\text{H}_2\text{O}$ (1 g; 4.13 mmol; 1.00 eq.) was dissolved in 75 mL of deionized water in a 200 ml beaker and stirred at 400 rpm to produce a clear, 0.55 M solution. In a separate 200 ml beaker $\text{CoCl}_2 \cdot 6\text{H}_2\text{O}$ (0.983 g, 4.13 mmol, 1.00 eq.) was dissolved in 75 mL of water to produce a 0.55 M solution as well. The $\text{CoCl}_2 \cdot 6\text{H}_2\text{O}$ solution was slowly added to the solution of $\text{Na}_2\text{MoO}_4 \cdot 2\text{H}_2\text{O}$ while stirring. The resulting solution was stirred in ambient for 4 hours. The solid product was then isolated on a cellulose acetate membrane filter (0.2 μm pore diameter, Sartorius) from the aqueous solution *via* vacuum filtration and washed with 1 L of water. The resulting powder (proved as a phase pure CoMoO_4 by XRD) was dried overnight on the filter in ambient and used without any additional temperature treatment.

Stoichiometric amounts of $\text{Co}(\text{OH})_2$ and CoMoO_4 (or MoO_3 only in case of making a pure Mo) powders were mixed together with pestle and mortar. The powder mixture was sandwiched between two silica wool pieces inside a silica tube (8 mm diameter and 20 mm long). The silica tube was then placed inside a tube furnace which was put under the flow of 5 % H_2 in Ar.

Phase-pure Co_7Mo_6 was prepared in a single-step reaction between $\text{Co}(\text{OH})_2$ (8 mg, Alfa Aesar, 99.9 %) and CoMoO_4 (112.94 mg) for 10 hours at 950 °C in 5 % H_2 in Ar gas stream.

Phase-pure Co_3Mo was made in two steps. First, $\text{Co}(\text{OH})_2$ (84.92 mg, Alfa Aesar, 99.9 %) and CoMoO_4 (100 mg) were reacted at 700 °C for 10 hours in 5 % H_2 in Ar gas mixture. The resulting powder was reground with pestle and mortar, placed back into the silica tube and reannealed for 10 hours in 5 % H_2 in Ar gas mixture at 850 °C.

Mo metal was made by reduction of MoO_3 (Aldrich, 99.9 %) oxide in 5 % H_2 in Ar gas stream at 950 °C for 10 hours.

Co metal was prepared by heating $\text{Co}(\text{OH})_2$ in 5 % H_2 in Ar stream at 350 °C for 5 hours.

2.2. Materials characterisation

Powder X-ray diffraction (PXRD) was carried out on a Panalytical Xpert-Pro diffractometer with the Cu K α ($\lambda = 1.54184 \text{ \AA}$) source operating in the Bragg-Brentano geometry. A sample was carefully spread over a zero-background holder and flattened with a glass slide.

Scanning Electron Microscopy (SEM) was performed using a Phillips XL30 ESEM instrument equipped with an Oxford Instruments X-act spectrometer for Energy Dispersive X-ray Spectroscopy EDXS measurements. The INCA software was used for the data analysis. Cu foil was used as the calibration standard for the EDXS. The sample preparation involved dispersing *ca.* 1 mg of alloy powder in 1 ml of hexane on sonication for 5 minutes. 100 μl drop of resulting solution was casted on Cu foil producing a well-spread and homogenous coating.

2.3. Electrochemical characterisation

Electrocatalysts were prepared in the form of inks, which were loaded onto polished glassy carbon electrodes, for catalytic testing. To prepare the catalytic ink: 8 mg of a synthesised catalyst was added to a mixture of 1.00 mL of DMF and 50 μL of Nafion followed by sonication for half an hour. 30 μL of the prepared inks were applied onto the surface of polished glassy carbon electrodes with a surface area of 0.071 cm^2 (corresponding to sample loading of *ca.* 3.3 $\text{mg cm}^{-2\text{geometric}}$) and then left to dry overnight. A Biologic SP-150 potentiostat with a three-electrode setup was used to investigate the electrochemical performance. The prepared electrode was used as a working electrode, and carbon felt and 3M Ag/AgCl were used as counter and reference electrodes, respectively. The catalytic activity towards the HER was tested in 0.5 M H_2SO_4 and 1 M KOH for all materials. The electrode potentials were converted to RHE by $E(\text{RHE}) = E(\text{Ag}/\text{AgCl}) + 0.209\text{V} + 0.059 \times \text{pH}$ value and the ohmic resistances were compensated. Polarization curves were obtained using linear sweep voltammetry (LSV) and cyclic voltammetry were set up in a single compartment electrochemical cell and were performed with a scan rate of 5 mV s^{-1} and 100 mV s^{-1} . Tafel plots were obtained from the polarisation data.

3. Results and Discussion

Initial attempts were made to make Co_3Mo from CoMoO_4 as described in [11]. However, only formation of Co_7Mo_6 with Mo as an impurity (in line with the nominal Co : Mo = 1 : 1 composition in CoMoO_4) was observed within tested temperature ranges of 700 – 950 $^\circ\text{C}$. Therefore, the reaction of mixtures of CoMoO_4 and $\text{Co}(\text{OH})_2$ was used instead of a single CoMoO_4 precursor. This proved to be a successful strategy for synthesis and gave phase pure products. Therefore, all samples reported in this work were made by this route as also described in the experimental section.

The PXRD pattern of Co_3Mo (Fig. 1a) prepared at 850 $^\circ\text{C}$ shows a very good match with the simulated patterns for hexagonal Co_3Mo . The attempts to prepare Co_3Mo at higher temperatures (to match the reaction temperature with the one used for synthesis of Co_7Mo_6 for a better comparison between two alloys) led to phase separation with Co and Co_7Mo_6 as impurities. Therefore, the temperature of 850 $^\circ\text{C}$ was deemed optimal. The attempt to carry out the reaction at higher temperatures was motivated by assumption that the products prepared at similar temperature are more likely to have similar morphologies and surface areas. Hence, a comparatively more reliable assessment of their electrochemical performance would be possible.

The formation of phase pure rhombohedral Co_7Mo_6 was only successful at relatively high temperature of 950 $^\circ\text{C}$ as evident from the powder X-ray diffraction which matched very well with the peak positions of the simulated pattern for Co_7Mo_6 from the ICSD. The lower intensity of some peaks especially the peak at *ca.* 42.5 $^\circ$ when compared with the simulated pattern was probably due to peak broadening caused by disorder (stacking faults) within the rhombohedral structure of Co_7Mo_6 [13]. Lower reaction temperatures used for synthesis of Co_7Mo_6 always resulted in elemental Mo impurities.

Attempts to synthesize Co_2Mo_3 using CoMoO_4 and MoO_3 (which appeared as a logical extension to Co_3Mo and Mo_7Co_6 series) invariably led to a phase mixture of Mo_7Co_6 and elemental metal Mo.

The reader may have noticed from the experimental part that both Co and Mo used as controls were prepared by reduction in H_2/Ar stream from $\text{Co}(\text{OH})_2$ and MoO_3 (rather than using elemental Co

and Mo purchased from the suppliers of chemicals). The rationale behind this approach was based on an assumption that it would provide a more adequate comparison with alloys which were made under reductive conditions from CoMoO_4 and $\text{Co}(\text{OH})_2$.

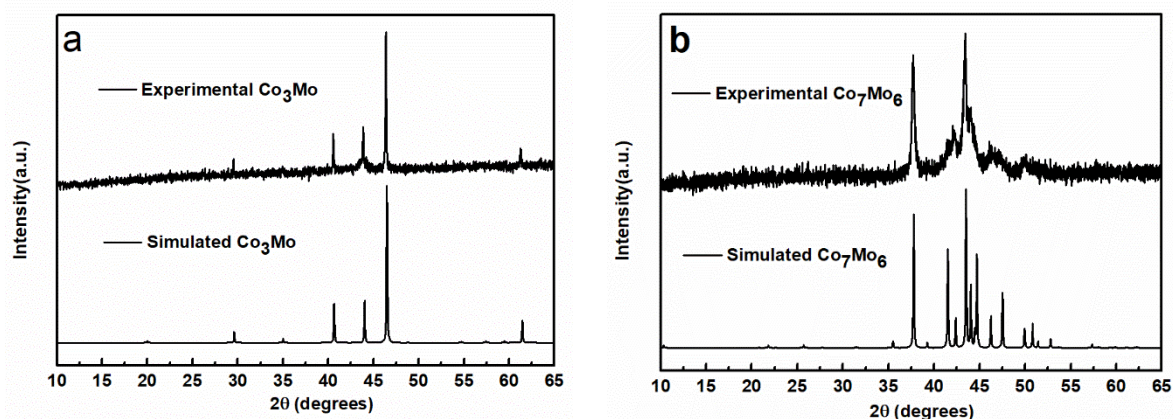


Figure 1. Powder X-ray diffraction (PXRD) of phase pure alloys: (a) Co_3Mo prepared at 850 °C and matched against simulated pattern from ICSD database (624214) (b) Co_7Mo_6 prepared at 950 °C matched against simulated pattern from ICSD database (624213).

The morphology of Co_3Mo from the SEM (Fig. 2a) could be described as consisting of spherical-shaped particles with a diameter of ca. 300 – 500 nm. The microstructure of Co_3Mo is substantially different from the morphology of CoMoO_4 precursor which consisted of well-defined prismatic microcrystals (Fig. S1). On the other hand, there is a certain degree of similarity between the morphology of Co_3Mo synthesized in this work and Co_3Mo prepared on Cu-substrate by dealloying Cu from an arc-melted product in sulfuric acid [12].

Co_7Mo_6 showed similar microstructure as Co_3Mo although with less defined crystallite shapes and less apparent surface roughness (Fig. 2b). This similarity between Co_3Mo and Co_7Mo_6 surfaces is even more pronounced at lower magnification (Fig. S2) with Co_3Mo appearing more porous. The difference is unsurprising given that the higher synthetic temperature was used for Co_7Mo_6 which could lead to sintering and coalescence of particles

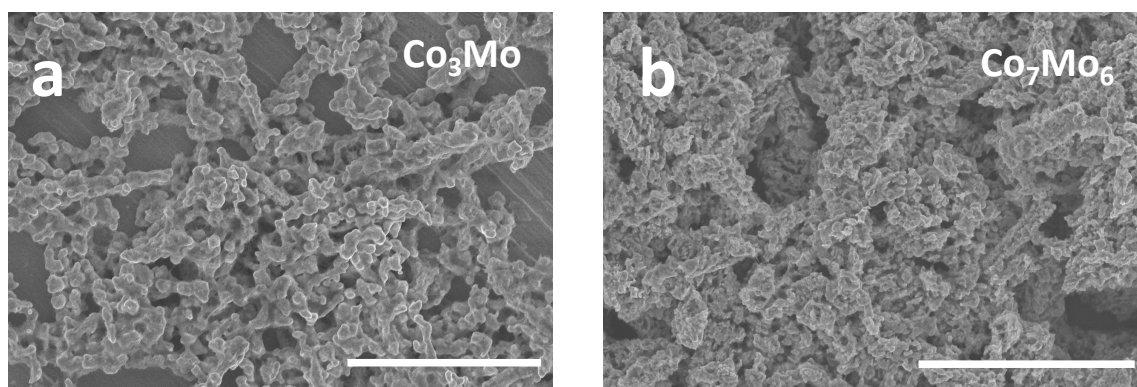


Figure 2. Scanning electron microscopy (SEM) images of Co_3Mo and Co_7Mo_6 : (a) Co_3Mo prepared at 850 °C (b) Co_7Mo_6 prepared at 950 °C. The scale bars on both graphs correspond to 5 μm .

Energy dispersive X-ray spectroscopy (EDXS) confirmed that Co_3Mo and Co_7Mo_6 are homogenous. The average compositions are in line with the expected theoretical compositions within the error of the measurements. The minor excess of Mo within the samples could be explained by the overlap between Cu (0.93 eV, L_{α}) and Co (0.76 eV, L_{α}) peaks (Fig. S3). The Cu-peak was due to the X-

ray beam penetrating down to Cu foil which was used as a support for drop-casted sample in EDXS characterization.

Table 1. Elemental analysis of Co_3Mo and Co_7Mo_6 by EDXS. The results are the average of values collected in several points across a sample and the errors present the standard deviations between the values at these points.

	Co_3Mo		Co_7Mo_6	
	Co	Mo	Co	Mo
at. % Exp.	73.57 ± 1.79	28.5 ± 2.1	50.55 ± 0.82	49.5 ± 0.82
at. % Theory	75	25	53.8	46.2

After establishing the purity of the samples linear sweep voltammetry (LSV) was used to investigate electrocatalytic activity of Co_3Mo and Co_7Mo_6 (Fig. 3a). At the current density of 10 mA cm^{-2} (which has been suggested as a useful benchmark in conjunction with photovoltaic applications [5]) the overpotential values of $115 \pm 8 \text{ mV}$ and $160 \pm 5 \text{ mV}$ are achieved for Co_3Mo and Co_7Mo_6 respectively (Fig. 3a). At the same current density Mo and Co show significantly higher overpotentials of $373 \pm 7 \text{ mV}$ and $411 \pm 5 \text{ mV}$ respectively. Furthermore, upon application of a reductive bias in $0.5 \text{ H}_2\text{SO}_4$ both alloys achieved much higher current densities (Fig. S4) than elemental Co and Mo powders. The observed overpotentials confidently place both Co_3Mo and Co_7Mo_6 among the best catalysts for HER from water in acidic electrolytes [5].

Tafel plots were studied to investigate the possible kinetics of the reaction (Fig 3b). However, the resulting Tafel slope values of $71 \pm 7 \text{ mV dec}^{-1}$ (Co_3Mo) and $84 \pm 5 \text{ mV dec}^{-1}$ (Co_7Mo_6) are outside the values for defined reaction mechanisms, *i.e.* 40 mV dec^{-1} (Volmer-Heyrovsky) and 120 mV dec^{-1} (Volmer) [5]. The deviation from ideal Tafel slopes is a common situation with powdered materials and Co_3Mo in particular [5, 11] as they do not always follow a perfect charge-transfer behaviour (Tafel behaviour) due to mass transport effects [14]. Proper accounting for mass transport effects requires comprehensive numerical simulation procedures which are beyond the scope of this manuscript.

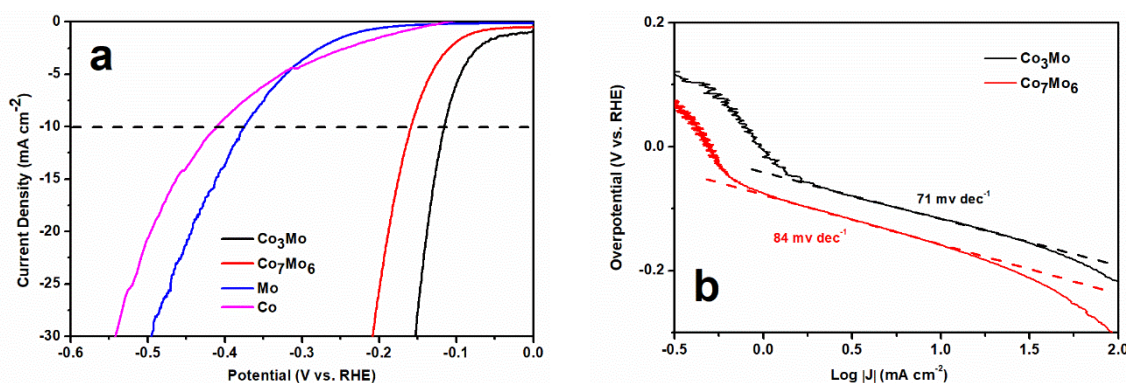


Figure 3. Electrochemical studies of Co_3Mo and Co_7Mo_6 : (a) Comparison of current densities achieved by Co_3Mo , Co_7Mo_6 as well as Mo and Co powders in $0.5 \text{ M H}_2\text{SO}_4$. The dashed line is guide to the eye at 10 mA cm^{-2} (b) Tafel plots and corresponding Tafel slopes of Co_3Mo and Co_7Mo_6 in $0.5 \text{ M H}_2\text{SO}_4$. Catalysts were prepared on a glassy carbon working electrode as described in the experimental section. Carbon felt and 3 M Ag/AgCl were used as the counter and reference electrodes, respectively.

An initial assessment of morphology by SEM indicated a denser Co_7Mo_6 sample. This could lead to a relative underperformance of Co_7Mo_6 in comparison with more porous Co_3Mo due to a lower surface area which leads to a lower specific activity [14]. Although we attempted the measurements of surface area using N_2 gas adsorption, the sorption characteristics of both samples were below the detection limit of the instrument due to the low surface area of the samples. Alternative option would be to investigate the surface area using Kr gas instead of N_2 which has been shown as an efficient

approach in case of Ni-Mo alloys [15]. However, our group lacks access to such equipment. Therefore, we used the values of double-layer capacitance (C_{DL}) for the comparison of the relative surface areas between two alloys. C_{DL} has been deemed to be proportional to roughness factor and therefore, is routinely used as an approximation for the electrochemical surface area of a sample in the absence of direct physical data [16, 17]. The C_{DL} values were evaluated at a constant potential from the difference of current densities with the scan rate (Fig. 4a). The ratio between $C_{DL}(\text{Co}_3\text{Mo}) : C_{DL}(\text{Co}_7\text{Mo}_6) = 2.7$ indicates that the surface area of Co_3Mo could be three times higher than that of Co_7Mo_6 ; although in the absence of direct measurements of surface area (such as gas sorption) this value should be treated with a great caution [18]. For example, Csernica *et al.* noticed that although the ratio between Kr BET surface area of their Mo_7Ni_7 and $\text{Ni}_{0.92}\text{Mo}_{0.08}$ varied almost by a factor of 4; the C_{DL} ratio between these sample was only 1.6 [15]. Still, in the absence of Kr BET data comparison between C_{DL} numbers appears as a good approximation as it seems to give the numbers of the same magnitude as BET data. The comparison of C_{DL} also corroborates with SEM result which pointed out that Co_3Mo is more porous than Co_7Mo_6 . Therefore, given the fact that the mass loadings and electrode surface area were identical, we can assume that the relative surface area of Co_3Mo is 2.7 lower than Co_7Mo_6 . Thus, the specific activity of Co_7Mo_6 ($\text{mA cm}^{-2}_{\text{catalyst}}$) is 2.7 times higher. In other words, based on this approximation Co_7Mo_6 can deliver 2.7 times higher current densities as demonstrated in Fig. S6 which also leads to an improved overpotential of 123 mV at 10 mA cm^{-2} . It is an interesting result especially given that the recent DFT calculations on Co_3Mo have shown that Mo-atoms are the catalytic sites in Co_3Mo [11]. One can assume that increasing the amount of Mo would lead to improve catalytic performance. However, due to differences in crystal structures of Co_3Mo and Co_7Mo_6 it is hard to draw definitive conclusions at this stage and further computational studies are required.

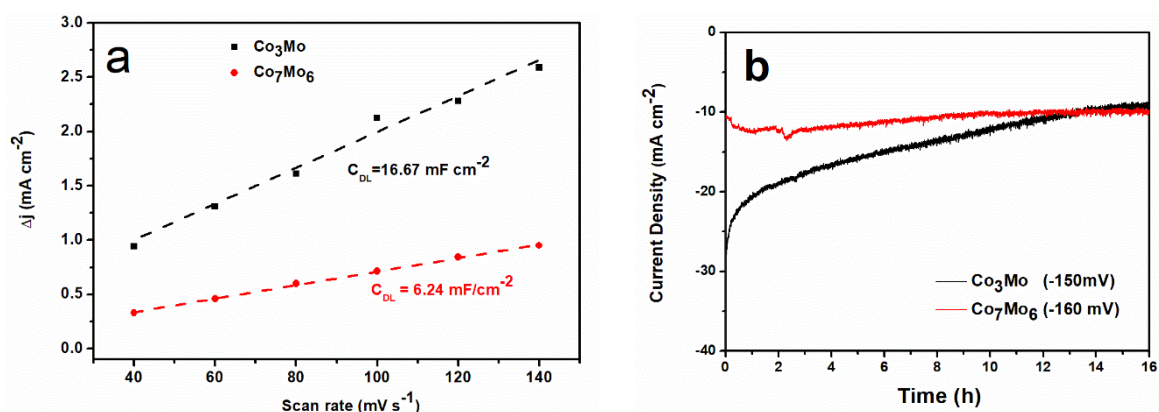


Figure 4. Evaluation of double-layer capacitance and stability of Co_3Mo and Co_7Mo_6 : (a) Current densities differences of Co_3Mo and Co_7Mo_6 plotted against scan rates. The capacitance currents were measured at 300 mV *vs.* NHE (b) Controlled-potential chronoamperometry profiles of Co_3Mo and Co_7Mo_6 in 0.5 M H_2SO_4 at the applied potentials of 150 and 160 mV respectively. Experiments were performed using a three-electrode setup, with catalyst-deposited glassy carbon as the working electrode, 3 M Ag/AgCl as the reference and carbon felt as the counter electrode. Catalysts were prepared on a glassy carbon working electrode as described in the experimental section. Carbon felt and 3 M Ag/AgCl were used as the counter and reference electrodes, respectively.

The stability of the catalysts was tested by applying a constant potential over time (Fig. 4d). There is a clear decline in current densities for Co_3Mo while Co_7Mo_6 retained the original values over 16 hours of testing without any evidence for decay. Co_7Mo_6 also shows a good stability upon cycling for 1000 times to the current densities of over 100 mA cm^{-2} at a scan rate of 100 mV s^{-1} (Fig. S7).

To the best of our knowledge this is a first report of electrocatalytic performance of Co_6Mo_7 and therefore, it is important to prove that the LSV measurements correspond to the actual reduction of protons to hydrogen. A representative trace of gas produced in an airtight cell and probed by gas chromatography is shown in Fig. S8, which confirmed the production of hydrogen using Co_7Mo_6 .

There are currently no electrochemical studies of Co_3Mo in acidic conditions and to the best of our knowledge no studies of Co_7Mo_6 in acidic or alkaline media. Therefore, to put the results into a perspective we studied Co_3Mo and Co_7Mo_6 by LSV in 1M KOH (Fig. S9). Both alloys show overpotentials of 120 ± 5 mV (Co_3Mo) and 160 ± 5 mV (Co_7Mo_6) at 10 mA cm^{-2} . In comparison with recently reported Co_3Mo on nickel foam the observed overpotential seems high [11]. Chen *et al.* showed overpotentials of 78 mV ($C_{\text{DL}} = 15.8 \text{ mF cm}^{-2}$) and 75 mV ($C_{\text{DL}} = 17.5 \text{ mF cm}^{-2}$) which are in good agreement to $C_{\text{DL}} = 16.64 \text{ mF cm}^{-2}$ observed in this work. The comparison points out the limitation of using double-layer capacitance (C_{DL}) as a proxy for the catalytic surface area. Without direct methods for measuring surface area it is hard to tell whether it is the substrate or other factors that led to such a difference in the overpotential values at the same C_{DL} . Still C_{DL} is a useful parameter as at least it provides some background information that enables a comparison between samples prepared in different labs. For example, Co_3Mo prepared by arc-melting showed overpotential of 340 mV at 10 mA cm^{-2} in 1M KOH [19] but as this work is missing C_{DL} values it is difficult to explain such a high value for overpotential. Conversely, nanoporous Co_3Mo on Cu substrate with a $C_{\text{DL}} = 324 \text{ mF cm}^{-2}$ achieved 65 mV cm^{-2} at 100 mA cm^{-2} [12]. Given the Tafel slopes of 40 mA cm^{-2} it suggests an overpotential of just 25 mV cm^{-2} at 10 mA cm^{-2} in 1M KOH. Therefore, it is often difficult to decouple the role of the substrate and morphology from the actual performance of the material and more research on free-standing catalysts is needed. Remarkably, on 1 M KOH Co_7Mo_6 achieved substantially higher current densities (well in excess of 120 mA cm^{-2}) than in $0.5 \text{ H}_2\text{SO}_4$ (Fig. S10). It also outperformed Co_3Mo as well as Co and Mo powders.

We also studied Tafel plots of Co_3Mo and Co_7Mo_6 (Fig. S11) which showed the Tafel slopes of 117 mV dec^{-1} (Co_3Mo) and 106 mV dec^{-1} (Co_7Mo_6) suggesting that the electron transfer reaction leading to H-adsorption on the surface of the catalyst is rate determining step [5]. The Tafel slope for Co_3Mo is broadly consistent with arc-melted Co_3Mo (105 mV dec^{-1}) [19] and Co_3Mo on Ni-foam [11] although it should be noted that in [11] the Tafel slopes varied quite significantly depending on the synthesis reaction times and C_{DL} values. Conversely, nanostructured Co_3Mo on Cu substrate [12] showed substantially different Tafel slope of 40 mV dec^{-1} [12]. This reinforces that the morphology and support material could play a vital role as well as adding an extra layer of complexity when it comes to comparison between products made in different labs.

Finally, we also evaluated the stability of Co_3Mo in 1M KOH to see how it compares with the products prepared on metal supports (Fig. S12). Quite notably contrary to the previous reports [11, 12] highlighting good stability on Co_3Mo on Ni-foam and Cu substrate there is a clear fading of the current with time. This suggests that substrate plays a significant role and it is important to study free-standing systems (decoupled from the support) to provide a better general understanding of the actual catalyst's performance.

4. Conclusions

In conclusion, phase pure Co_3Mo and Co_7Mo_6 can be prepared through the reaction of stoichiometric amounts of $\text{Co}(\text{OH})_2$ and CoMoO_4 . The evaluation of electrochemical performance points out that Co_3Mo and Co_7Mo_6 in their free-standing form could routinely show a confident performance which is similar with previously studied classes of materials in acidic conditions. To the best of our knowledge this is a first report on activity of Co_7Mo_6 towards HER either in acidic or alkaline condition. When adjusted for the C_{DL} ratios Co_7Mo_6 demonstrated improved current densities and an overpotential of 123 mV tentatively suggesting that it can be as electrocatalytically active as Co_3Mo while showing a better stability in acidic media. However, without accounting for surface areas by other methods these results should be treated with caution. This highlights a set of challenges for researchers working on nanostructured catalysts. The issue is quite evident from the comparison between free-standing Co_3Mo investigated in this work and Co_3Mo fabricated on Ni-foam or Cu substrates when tested in 1M KOH. The estimation of surface area by direct physical methods (*i.e.* through gas adsorption which is independent of sample history, oxidation state and solvent effects) is strongly recommended for an adequate comparison between products made in different labs.

Computational studies are also promising for clarification whether the difference in comparative performance of Co₃Mo and Co₇Mo₆ fundamentally persist and these will be explored in our future work.

Supplementary Materials: Figure S1: SEM image of CoMoO₄ precursor. Figure S2: Low magnification SEM image of Co₃Mo and Co₇Mo₆. Figure S3: A representative EDXS spectrum of Co₃Mo sample. Figure S4: Comparison of current densities achieved by Co₃Mo, Co₇Mo, Co and Mo. Figure S5: Comparison of current densities achieved by Co₃Mo, Co₇Mo₆ and Co₇Mo₆ when adjusted for results of double-layer capacitance (C_{DL}). Figure S6: Magnified version of Fig.S4 Figure S7: Comparison of current densities achieved by Co₇Mo₆ in 0.5M H₂SO₄ before and after 1000 scans at the scan rate of 100 mv s⁻¹. Figure S8: A representative trace of the gas chromatographic analysis of the single-cell headspace during the electrolysis of Co₇Mo₆ Figure S9: Comparison of current densities achieved by Co₃Mo, Co₇Mo₆ as well as Mo and Co powders in 1M KOH. Figure S10: Extended range of the Graph S9 Figure S11: Tafel plots and corresponding Tafel slopes of Co₃Mo and Co₇Mo₆ in 1M KOH. Figure S12:

Author Contributions: A.G. conceived and managed the experiments. Y.S. designed the experiments and carried them out. Y.S. and A.G. analysed and plotted the data. A.G. wrote the manuscript. All authors have read and agreed to the published version of the manuscript.

Funding: Parts of this research was funded by The Carnegie Trust for a Research Incentive Grant (RIG007428). China Scholarship Council (CSC) funded the CSC scholarship to Y.S.

Acknowledgments: A.G. acknowledges the Carnegie Trust for a Research Incentive Grant and the University of Glasgow for supporting this work. Y.S. thanks China Scholarship Council for providing him with the scholarship.

Conflicts of Interest: The authors declare no conflict of interests. The funders had no role in the design of the study; in the collection, analyses, or interpretation of data; in the writing of the manuscript, or in the decision to publish the results.

References

1. IEA *Global Energy Review 2020*, (2020) IEA, Paris. <https://www.iea.org/reports/global-energy-review-2020>. (accessed on 26 August 2020).
2. X. Fan, B. Liu, J. Liu, J. Ding, X. Han, Y. Deng, X. Lv, Y. Xie, B. Chen, W. Hu, C. Zhong, Battery Technologies for Grid-Level Large-Scale Electrical Energy Storage. *Trans. Tianjin Univ.* **2020**, *26*, 92–103.
3. IEA *The Future of Hydrogen*, (2019) IEA, Paris. <https://www.iea.org/reports/the-future-of-hydrogen> (accessed on 26 August 2020).
4. A. Buttler, H. Spliethoff, Current status of water electrolysis for energy storage, grid balancing and sector coupling via power-to-gas and power-to-liquids: A review. *Renew. Sustain. Energy Rev.* **2018**, *82*, 2440–2454.
5. I. Roger, M. A. Shipman, M. D. Symes, Earth-abundant catalysts for electrochemical and photoelectrochemical water splitting. *Nat. Rev. Chem.* **2017**, *1*, 1–13.
6. C. A. C. Sequeira, D. S. P. Cardoso, L. Amaral, B. Šljukić, D. M. F. Santos, On the performance of commercially available corrosion-resistant nickel alloys: A review. *Corros. Rev.* **2016**, *34*, 187–200.
7. A. Keçebaş, M. Kayfeci, M. Bayat, In *Solar Hydrogen Production: Processes, Systems and Technologies*; Elsevier, 2019; pp. 299–317.
8. A. Kongkanand, M. F. Mathias, The Priority and Challenge of High-Power Performance of Low-Platinum Proton-Exchange Membrane Fuel Cells. *J. Phys. Chem. Lett.* **2016**, *7*, 1127–1137.
9. M. M. Jaksic, Hypo-Hyper-d-Electronic Interactive Nature of Interionic Synergism in Catalysis and Electrocatalysis for Hydrogen Reactions. *Int. J. Hydrogen Energy* **2001**, *26*, 559.
10. J. G. Highfield, E. Claude, K. Oguro, Electrocatalytic Synergism in Ni/Mo Cathodes for Hydrogen Evolution in Acid Medium: A New Model. *Electrochim. Acta* **1999**, *44*, 2805.
11. J. Chen, Y. Ge, Q. Feng, P. Zhuang, H. Chu, Y. Cao, W. R. Smith, P. Dong, M. Ye, J. Shen, Nesting Co₃Mo Binary Alloy Nanoparticles onto Molybdenum Oxide Nanosheet Arrays for Superior Hydrogen Evolution Reaction. *ACS Appl. Mater. Interfaces* **2019**, *11*, 9002.
12. H. Shi, Y. T. Zhou, R. Q. Yao, W. Bin Wan, X. Ge, W. Zhang, Z. Wen, X. Y. Lang, W. T. Zheng, Q. Jiang, Spontaneously Separated Intermetallic Co₃Mo from Nanoporous Copper as Versatile Electrocatalysts for Highly Efficient Water Splitting. *Nat. Commun.* **2020**, *11*, 1.

13. J. Sort, S. Suriñach, S. Muñoz, D. Baró, M. Wojcik, E. Jedryka, S. Nadolski, N. Sheludko, J. Nogués, Role of Stacking Faults in the Structural and Magnetic Properties of Ball-Milled Cobalt. *Phys. Rev. B - Condens. Matter Mater. Phys.* **2003**, *68*, 014421.
14. D. Li, C. Batchelor-McAuley, R. G. Compton, Some thoughts about reporting the electrocatalytic performance of nanomaterials. *Appl. Mater. Today* **2020**, *18*, 100404.
15. P. M. Csernica, J. R. McKone, C. R. Mulzer, W. R. Dichtel, H. D. Abruña, F. J. DiSalvo, Electrochemical Hydrogen Evolution at Ordered Mo₇Ni₇. *ACS Catal.* **2017**, *7*, 3375.
16. D. Voiry, M. Chhowalla, Y. Gogotsi, N.A. Kotov, Y. Li., R.M. Penner, R.E. Schaak, P.S. Weiss, Best Practices for Reporting Electrocatalytic Performance of Nanomaterials *ACS Nano* **2018**, *12*, 9635–9638.
17. J. D. Benck, T. R. Hellstern, J. Kibsgaard, P. Chakthranont, T. F. Jaramillo, Catalyzing the hydrogen evolution reaction (HER) with molybdenum sulfide nanomaterials. *ACS Catal.* **2014**, *4*, 3957–3971.
18. S. Trasatti, O. A. Petrii, Real surface area measurements in electrochemistry. *J. Electroanal. Chem.* **1992**, *327*, 353–376.
19. Y. Li, X. Ge, L. Wang, J. Liu, Y. Wang, L. Feng, A Free Standing Porous Co/Mo Architecture as a Robust Bifunctional Catalyst toward Water Splitting. *RSC Adv.* **2017**, *7*, 11568.